Article:
Mertes, JR, Thompson, SS, Booth, AD et al. (2017) A conceptual model of supraglacial lake formation on debris-covered glaciers based on GPR facies analysis. Earth Surface Processes and Landforms, 42 (6). pp. 903-914. ISSN: 0197-9337

https://doi.org/10.1002/esp.4068

Title

A conceptual model of supraglacial lake formation on debris-covered glaciers based on GPR facies analysis.

Authors

Jordan R. Mertes[1,2], Sarah S. Thompson[2], Adam D. Booth[3], Jason D. Gulley[4], Douglas I. Benn[5]

Affiliations

[1] Department of Geological and Mining Engineering and Sciences, Michigan Technological University, 630 Dow Environmental Sciences, 1400 Townsend Drive, Houghton, MI 49931, USA

E-mail: JRMertes@mtu.edu

[2] Department of Arctic Geology, University Centre in Svalbard, Postboks 156, NO-9171, Longyearbyen, Svalbard, Norway

E-mail: Jordan.Robert.Mertes@unis.no

[3] School of Earth and Environment, University of Leeds, Leeds, LS2 9JT, UK

[4] School of Geosciences, University of South Florida, 4202 E. Fowler Avenue, NES 107, Tampa, FL 33620-5550 USA

[5] School of Geography and Geosciences, University of St. Andrews, North Street, St. Andrews, Fife KY16 8ST, UK

This article has been accepted for publication and undergone full peer review but has not been through the copyediting, typesetting, pagination and proofreading process which may lead to differences between this version and the Version of Record. Please cite this article as doi: 10.1002/esp.4068

Abstract

Supraglacial lakes and ponds can create hotspots of mass loss on debris-covered glaciers. While much research has been directed at understanding lateral lake expansion, little is known about the rates or processes governing lake deepening. To a large degree, this knowledge gap persists due to sparse observations of lake beds. Here we report on the novel use of ground penetrating radar (GPR) surveys to simultaneously collect supraglacial lake bathymetry and bottom composition data from Spillway Lake (surface area of 2.4 x 10^5 m^2; volume of 9.5 x10^4 m^3), which is located in the terminus region of the Ngozumpa Glacier in the Khumbu region of the Nepal Himalaya. We identified two GPR bottom signals corresponding to two sedimentary facies of (1) sub-horizontal layered fine sediment drape and (2) coarse blocky diamict. We provide an understanding of the changes in subaqueous debris distribution that occur through stages of lake expansion by combining the GPR results with *in situ* observations of shoreline deposits matching the interpreted facies. From this, we present an updated conceptual model of supraglacial lake evolution, with the addition of data on the evolving debris environment, showing how dominant depositional processes can change as lakes evolve from perched lakes to multi-basin base-level lakes and finally onto large moraine-dammed lakes. Throughout lake evolution, processes such as shoreline steepening, lakebed collapse into voids and conduit interception, subaerial and subaqueous calving and rapid areal expansion alter the spatial distribution and makeup of lakebed debris and sediments forcing a number of positive and negative feedbacks on lake expansion.

Introduction

Thick layers of debris on debris-covered glacier tongues have been found to insulate debris-covered glaciers from mass loss in response to climate warming by decreasing heat flux to the underlying ice surface (Østrem, 1959, Nakawo and Rana, 1999, Nicholson and Benn, 2006, Reid and Brock, 2010, Reznichenko, et al., 2010, Shea and Immerzeel, 2016). However, mass loss on some debris-covered glaciers has been shown to be keeping pace with adjacent clean ice glaciers (Gardelle, et al., 2012, Kääb, et al., 2012). This phenomenon may be attributed to irregular surface evolution due to uneven sub-debris melting leading to the presence of features such as supraglacial lakes and ice cliffs, which act as localized hotspots of melting. In some cases, these hotspots have been shown to contribute to mass loss significantly, though only making up a very small part of the glacier surface area (Sakai, et al., 2000b, Sakai, et al., 2002, Reid and Brock, 2014, Buri, et al., 2015, Miles, et al., 2016, Thompson, et al., 2016). Through time however, the growth of supraglacial lakes and the rapid backwasting of bordering ice cliffs, can eventually lead to coalescence with nearby lakes, and increased chances to form potentially dangerous moraine-dammed lakes (Sakai, et al., 2000a, Watanabe, et al., 2009).

Supraglacial lakes contribute to glacier mass loss by driving melt in the tongues of stagnant, debris-covered glaciers where surface slopes are generally < 2° (Reynolds, 2000, Sakai, et al., 2002, Immerzeel, et al., 2014, Reid and Brock, 2014, Thompson, et al., 2016). With low glacier surface slopes, meltwater and rainfall accumulate in topographic depressions where they contribute to melt by absorbing and storing incoming radiation as heat (Kirkbride, 1993, Benn, et al., 2000, Reynolds, 2000, Sakai, et al., 2000b, Benn, et al., 2001, Röhl, 2008, Miles, et al., 2016). Circulation of warm lake water increases melt around lake margins and stored

heat drives subaqueous melting, even when ambient temperatures have decreased below freezing (Sakai, et al., 2000a). In addition to melt within lake basins, interception with englacial conduits can transfer warm water to the interior of the glacier contributing to internal ablation (Kirkbride, 1993, Benn, et al., 2012, Miles, et al., 2016, Thompson, et al., 2016).

Much of what is known about the evolution of supraglacial lakes concerns areal expansion and the rates and fundamental processes underpinning areal lake expansion are well established from remote sensing and surface surveys (Mool, 1995, Quincey, et al., 2007, Komori, 2008, Fujita, et al., 2009, Watanabe, et al., 2009, Bajracharya and Mool, 2010, Gardelle, et al., 2011, Sawagaki, et al., 2012, Thompson, et al., 2012, Liu, et al., 2015, Wang, et al., 2015, Thompson, et al., 2016). Far less, however, is known about rates of, and processes controlling, lake deepening. To a large degree, this is because the remote sensing techniques used to measure lake depth on clean ice glaciers (Sneed and Hamilton, 2007, Fitzpatrick, et al., 2014), where lakes are clear, do not work in the turbid lakes that are characteristic of debris-covered glaciers. As a result, much of what is known about lake bathymetry has been determined from labor intensive field campaigns which have typically been conducted at irregular intervals.

While many details of lake deepening remain unknown, two physical processes are thought to dominate: subaqueous calving (Röhl, 2008) and direct lakebed melting (Chikita, et al., 1999, Sakai, et al., 2000b, Chikita, et al., 2001). Subaqueous calving has been observed to remove large volumes of ice from lake beds at a number of glaciers in New Zealand (Kirkbride and Warren, 1997, Warren and Kirkbride, 2003, Röhl, 2008). However, the mechanism relies in part on the buoyancy of ice and doubt remains as to the impact of the subaqueous debris layer (Benn, et al., 2012).

Melt rates of lakebeds are critically dependent on water temperature as well as the presence or absence of lake bed debris. For example, on the Lirung Glacier, Nepal, low subaqueous melt rates of < 0.01 cm d^{-1} occurred in lake beds covered in sediments, but where lakes were floored with bare ice, subaqueous melt rates were 2-4 cm d^{-1} (Miles, et al., 2016).

Improved understanding of the rates and processes of lake deepening requires a detailed temporal and spatial record of lake bathymetric evolution, as well as an understanding of debris distribution and physical characteristics. Most bathymetric survey techniques rely on weighted lines or hand-held electronic sonar devices (Yamada and Sharma, 1993, Kadota, 1994, Benn, et al., 2001, Sakai, et al., 2003, Yamada, et al., 2004, Sakai, et al., 2005, Fujita, et al., 2009, Sawagaki, et al., 2012, Thompson, et al., 2012, Somos-Valenzuela, et al., 2014, Horodyskyj, 2015, Thompson, et al., 2016). These techniques are time consuming and labor intensive, lack fine spatial resolution and provide little to no information about bottom compositions. Improved spatial resolution was obtained from surveys conducted using remotely operated underwater vehicles (ROVs) outfitted with sonar transducers (Horodyskyj, 2015), and sonar data can be analyzed to provide some information about bottom hardness and texture (Kenny, et al., 2003) but most commercial sonar systems cannot provide information about debris thickness.

Ground penetrating radar (GPR) is an underutilized tool for characterizing supraglacial lake bathymetry as well as bottom composition and thickness. While GPR has been used to measure glacier depths and ice volume for bathymetric and geological mapping of non-supraglacial lakes (Haeni, et al., 1987, Sellmann, et al., 1992, Moorman and Michel, 1997, Schwamborn, et al., 2002, Arcone, et al., 2006,

Banks and Johnson, 2011, Sambuelli and Bava, 2012), few studies have used GPR to investigate lakes on debris-covered glaciers (Reynolds, 2011).

In this paper we present the results of GPR surveys of Spillway Lake, Ngozumpa Glacier, Nepal to demonstrate the potential of GPR as an investigative tool for characterization of supraglacial lake bathymetry and lake bed characteristics. We then use a combination of GPR facies analysis (e.g.,Bristow, 1995, Ruffell, et al., 2004) and field observations to characterize and interpret the subaqueous debris distribution. Finally, we present an updated conceptual model of debris-covered glacier supraglacial lake evolution that is based on the facies analysis and a review of published literature on supraglacial lakes.

Study Site

Ngozumpa Glacier (27.97°N; 86.69°E) is located in the Khumbu Himal, Nepal, ~25 km west of Sagarmatha (Mt. Everest). The Ngozumpa Glacier flows down from Gyachung Kang (to the northeast) and Cho Oyu (to the northwest) (Fig 1). At ~20 km long, the glacier is one of the largest in Nepal, and the lower 15 km is extensively debris covered. Debris thickness is highly variable but generally increases from a thin, discontinuous cover just below the equilibrium line altitude (~5700 m) to the terminus, where it is continuous (excluding ice cliffs) and 1-3 m thick (Benn, et al., 2012, Nicholson and Benn, 2012). This debris layer has affected the glacier mass balance and altered the distribution of ablation relative to a clean ice glacier; the maximum ablation now occurs up glacier from the terminus where the debris layer is thin, rather than at the terminus. This ablation pattern has caused a reduction in surface gradient and an associated decrease in the driving stresses (Bolch, et al., 2008, Quincey, et al., 2009). In recent decades the glacier has experienced

substantial surface lowering, and, in the ablation area, the surface now lies >150 m below the Little Ice Age moraines (Sakai and Fujita, 2010). Decreases in surface gradient and driving stresses have ultimately led to a reduction in glacier velocity which has caused the lower ~7 km of the glacier to become stagnant (Quincey, et al., 2009, Thompson, et al., 2016).

The glacier has highly variable surface topography, consisting of large hummocks, ridgelines, lakes and ice cliffs. The surface relief is approximately 10s of meters around larger hummocks and lake ice cliff contacts. The mean surface slope of the lowest 5km has been measured previously at ~2° (Hands, 2004). This slope is within the range cited as having potential for the formation of extensive supraglacial lakes (i.e. ≤2°) (Reynolds, 2000, Quincey, et al., 2007, Röhl, 2008) and in the lowest ~2km where our study focuses, the overall slope decreases to <1°.

In the early 1990s a collection of lakes and ponds began to form at the hydrological base level of the Ngozumpa Glacier (Thompson, et al., 2012). Since this time, the lake basins have continued to grow and coalesce to cover an area of 2.4 x 10^5 m^2 with a volume of 9.5 x10^4 m^3 in 2014 (Thompson, et al., 2016). This growing lake body is, informally, referred to as Spillway Lake. The site has been the focus of a series of studies using remote sensing, sonar measurements and extensive field mapping (Adhikary, et al., 2000, Benn, et al., 2001, Benn, et al., 2012, Thompson, et al., 2012, Horodyskyj, 2015, Thompson, et al., 2016). Our new surveys, presented here, focus on two connected basins within the Spillway Lake system, adjacent to the eastern lateral moraine and the central lake basin (Fig 2 A, B).

Methods

During December 2014, five GPR transects were surveyed on the frozen surface of Spillway Lake, using a Malå ProEx Professional Explorer GPR system linked to an unshielded Rough Terrain Antenna (RTA) of 25 MHz center frequency. The RTA is roughly 13 m long and houses a single pair of transmitter/receiver antennas separated by 6 m in an inline configuration. During acquisition, the system was connected to a Leica Differential Global Positioning System (DGPS) rover, and set to record a trace every 0.3 s. The ProEX unit was placed inside an inflatable kayak behind which the RTA was towed. The system was towed on foot at an approximately constant speed of ~1 m s^{-1}. The interval between recorded traces was 0.26 ± 0.06 m, regularized (in Mathworks Matlab® software) to 0.2 m during processing. A bulk correction of 11 m (applied in the opposite direction to the profile heading) was applied to all positions to remove the offset between the DGPS antenna and the midpoint between the GPR antennas. Due to a battery failure in the Leica base station, GPS measurements cannot be post processed and corrected to centimeter accuracy. Therefore, to assure the most accurate transect positioning, we have used field video and photographic data to verify correct positioning of transect start-stop positions relative to high-resolution satellite imagery (~ 0.48 m pan-sharpened GeoEye-1) where possible. Uncorrected DGPS data from sonar surveys, conducted prior to the GPR survey, show errors on the scale of ±1-2 m in the x-y plane.

The effective depth of investigation of a GPR signal is substantially impeded in electrically conductive ground (e.g., high clay fraction and/or saline water content) as the electromagnetic energy of the GPR wavelet is more rapidly absorbed (Annan, 2004). Groundwater is therefore often considered an impediment to GPR surveying.

Supraglacial lakes, however, can have very low electrical conductivities, with conductivities of ~2.3 mS m^{-1} to ~12 mS m^{-1} being reported from supraglacial lakes on debris-covered glaciers (Watanabe, et al., 1995, Sambuelli and Bava, 2012). These conductivities are close to pure water and lakes should thus be transparent to radar.

The RTA used to conduct our GPR surveys allows for rapid data acquisition, but it does not allow common midpoint (CMP) surveys to be conducted for velocity analysis. As a result, GPR surveys reported here do not provide information about lakebed debris thickness. They can, however, provide information about bottom composition and water depth based on the first arrival of the GPR signal and its character immediately thereafter. In the absence of CMP-derived velocities, we assume a relative dielectric permittivity, ε_r, for water of 80 (Annan, 1992). Surface ice cover is ~0.2 m thick; therefore, our time-to-depth conversions assume a GPR velocity of 3.3 x 10^{-2} mns^{-1} throughout. While ε_r can vary with temperature (e.g. Malmberg and Maryott (1956) measured $\varepsilon_r \approx 88$ at 0°C), the uncertainty in depth estimates is expected to be small and the difference in derived velocity, and therefore depth estimates, between ε_r values of 80 and 88 is < 5%. Hence, in the absence of lake water temperature measurements, we use $\varepsilon_r = 80$. We estimate the wavelength of the 25 MHz RTA wavelet to be 1.3 m; the ¼-wavelength criterion for vertical and (following migration) lateral resolution suggests that our limit of resolution is 0.3 m. Data processing steps, implemented in Sandmeier ReflexW© 7.5 software, are listed in Table 1. The data generally respond well to the imposed processing flow, although artefacts of normal moveout correction remain at early travel-times where the propagation path of GPR energy is comparable in length to the 6 m offset between the two antennas. Very few artefacts of migration remain;

those that do are presumably caused by off-line scatter, and cannot be correctly migrated given the 2D acquisition.

By picking the first-break of lakebed reflections, we calculated bathymetry for each trace of the GPR dataset. This operation was straightforward in the deepest sections of the lake but was subject to greater uncertainty in shallower sections where the bed reflection was generally more complex. Bed reflection characteristics are discussed in the Results section under “GPR Facies Classification”. In addition, the shallower areas are subject to distortions in our normal moveout correction (e.g. Fig 3, beginning of transect 1, A). Given the finite lateral resolution of the GPR wavelet, we picked bathymetry to be deliberately smooth, and estimate that the uncertainty in the calculation of lake depth to be at maximum ±1 m.

The performance of the GPR depth conversion is assessed against the results of a separate sonar bathymetry point survey performed in December 2014 using a Hummingbird 385ci DualBeam™ sonar (Thompson, et al., 2016). The grid spacing of sonar survey was ~20 m along track and 6-40 m between tracks (Fig 2), and results were spline interpolated with a shoreline polygon barrier in ESRI ArcMap to provide a map of lake bathymetry. However, because the sonar bathymetry survey was not conducted specifically for comparison with the GPR survey, the GPR survey lines do not directly overlap the sonar points. Thus, we expect there to be variability in the comparison and use this as a broad assessment of the GPR depth conversion, rather than an assessment of the superiority of methods. Sonar points located closer to the GPR profiles are likely to provide a better corroboration of the GPR data than those located at a greater distance. The source pulse of the echo-sounder blends frequencies of 85 and 200 kHz, which gives vertical and lateral resolution comparable to the GPR, assuming a sonic velocity of 1500 m s^{-1} in water. We

therefore extracted interpolated sonar depth estimates along the radar transects to provide the necessary comparison between the two platforms.

Finally, we used GPR facies analysis to classify the lakebed from the processed GPR data. Facies analysis (Bristow, 1995, Ruffell, et al., 2004) is a qualitative means of characterizing styles of reflectivity, thereby allowing the mapping of consistent features, which have similar reflection geometry. We applied this qualitative approach to classification, as a more quantitative analysis is not possible in the absence of CMP data.

Results

GPR bathymetry

In GPR transects from basin A (Fig 3; transects 1-4) and basin B (Fig 4), we interpret the first arrival after a transparent section of data to be the reflection from the lakebed. The maximum two-way travel-time of the lakebed reflection is ~ 1300 ns, corresponding to a maximum lake depth of ~ 21 m (Fig 3, transect 1). In Basin A, the lakebed geometry appears generally bowl-shaped, relatively flat in the deeper areas, sloping up to the shoreline at an angle of 20-30° relative to the lake surface. A prominent hummock occurs in the center of the basin in transects 1 and 3 (Fig 3). The hummock is inferred to be ~60 m wide at its base, with a topographic high point at a depth of ~ 9 m, ~ 16 m shallower than the surrounding lakebed. Transect 2 (Fig 3) also shows evidence of the hummock, but the shoreward slope is not well defined. In Basin B, lakebed geometry shows a gradual deepening from 1 m in the south to 6 m in the north over a distance of ~120 m, followed by rapid deepening to 15 m (Fig 4). The lake shallows again to depths of 3-7 m between distance of 220 m and 260

m along track. This section of the lake appears to have a more undulating bathymetry.

Comparison with sonar data

Only six of the sonar survey points are located within a distance of ≤1 m from the GPR transects. The mean difference between these sonar point depth measurements and the closest measured GPR depths was 1.4m (Fig 5a). Differences between the GPR depths and the interpolated sonar depths were generally larger, with positive differences ranging from 2.3 to 7.7 m and negative differences ranging from -1.1 to -6.0 m (Fig 5b). Transects 2A, 4A and 1B, which roughly follow grid lines of the sonar measurements, all have differences less than ±5m with mean differences and standard deviation of 1.2±1.2 m, -0.7±1.7 m and -0.8±1.4 m respectively (Fig 5b). Conversely, transects 1A and 3A, running oblique to sonar measurement grid, all have differences greater than 5 m and less than -4.3 m with means and standard deviations of -0.4±3.0 m and 1.2±3.8 m respectively (Fig 5b). The mean difference of all transects is 0.1 m, with a standard deviation of ±2.5 m.

GPR facies classification

Sediment appears to cover the entire surveyed parts of the lakebeds. Two facies can be distinguished based on the characteristics of the lakebed reflectors (Fig 6). Facies 1 shows coherent, sub horizontal reflectivity, with parallel events either side of incoherent responses (Fig 6a). Facies 1 is present in the deeper areas of both lake basins and around the lake flanks (Fig 3 and 4). Facies 2 shows low-amplitude,

chaotic reflectivity, characteristic of structural complexity (Fig 6b). Facies 2 is present mostly around the submerged hummocks in basin A as well as the eastern shallows of transect 4 A (Fig 3).

Interpretation and discussion

GPR analysis and interpretation

Differences in point depth measurements made using GPR and sonar are smallest where distances between the measurements were smallest (Fig 5a). Similarity of depth measurements results from the GPR and sonar having similar un-migrated horizontal resolutions, with a mean difference of 0.52 m over the depth ranges in our study. Differences between GPR depths and interpolated sonar depths are likewise smallest along transects that have the largest number of proximate sonar point measurements, as well as where lake bathymetry is relatively flat. For example, transects 2A, 4A and 1B appear very similar to the interpolated sonar depths (Fig 7). All three transects have a gradually changing bathymetry, with only a few regions of rapid change. GPR traces for these transects are located a mean distance of 8.4±2.8 m, 5.3±1.7 m and 7.2±3.5 m away from their nearest sonar point measurements respectively (Fig 8). The maximum and minimum distances for transects 2A and 4A are 12.9 – 2.6 m and 8.9 – 1.6 m respectively. Transect 1B, however, has a much larger range of distances with a maximum and minimum of 17.1 – 0.9 m. The mean distance to sonar measurements along Transects 1A and 3A is similar to that for Transect 2A, but the variability along these two transects is greater than for 2A, with maximum distances at 20.4 m and 20 m respectively (Fig 8).

The two sets of depth measurements become more divergent where lake bathymetry is more complex (e.g. Figure 7, transect 3A, 50-150 m) likely as the result of sparse point data to constrain interpolation. For example, the greatest differences between depth measurements occur in transects 1A and 3A, where point data are spaced further than 13 m apart (e.g. Fig 2 red ellipse) and interpolation errors are likely to be the greatest. Similarly, transect 1B shows small variation in differences, yet has numerous outliers (Fig 5b) that correspond to large distances from sonar point measurements (Fig 8). These locations of larger difference are easily identifiable in Figure 7 and seen as the central area of basin B where data are again sparse. Small differences in depth measurements using the two techniques indicate GPR provides depth information that is roughly equivalent to sonar, but GPR has the added advantages of rapid data acquisition when collected on frozen lake surfaces and provides information about lakebed composition and structure.

Facies

Facies 1 is consistent with a more uniform scattering in which discontinuities are much smaller than the radar wavelength (i.e. 1.3 m). We interpret these sub-parallel sequences of reflectivity as layers of fine sediment, similar to the bedded sand deposits exposed around some lake margins (Fig. 9, 1&2 (right)). By contrast, Facies 2 is consistent with a chaotically scattering lakebed where discontinuities are on a spatial scale comparable with the radar wavelength (i.e., 1.3 m). We interpret Facies 2 as areas of the lakebed covered with coarse debris, including boulders and large clasts, similar to the widespread blocky diamict debris cover exposed on the glacier surface (Fig. 9, 1&4). Our facies classifications and identification agree well with the mapped distribution of bottom surface types found by Horodyskyj (2015), and are

also consistent with the observation that bathymetry associated with Facies 1 is likely to have less abrupt changes than in areas where Facies 2 is found.

The lack of exposed ice in our lakebed surveys suggests that any bare ice in lake basins is rapidly covered by sediments. Facies sequences, however, suggest that bare ice is exposed at lakebeds at least transiently. For example, if Facies 2 is in contact with ice on the lakebed, it cannot be known if the sediments were deposited as part of a mass wasting event onto a bare ice bed following lake formation or if they reflect an original debris-covered ice surface that was submerged following surface downwasting. In contrast, because Facies 1 suggests deposition by settling of finer grained materials, the superposition of Facies 1 with glacier ice at the lake bed strongly suggests the lake bed consisted of bare ice likely present prior to Facies 1 deposition (Figs 9, 3&4; Fig 10). Facies relationships suggest that up 20% of our survey lines were initially composed of bare ice, but were later covered by Facies 1 sediments.

Overlapping facies relationships demonstrate that the dominant sediment/debris delivery mechanisms to lakes can switch from mass wasting, toppling from ice cliffs and/or sliding from moraine ridges to settling of suspended fines, creating a transition from Facies 2 to Facies 1. For example, the upward transition from Facies 2 to Facies 1 (Fig 3) between 130 and 160 m in transect 3A, and between 120 to 160 m in transect 2A, indicate that the dominant sediment delivery mechanism switched from mass wasting to deposition of fines. Such a transition would be expected to occur as lakes expanded. Sediments would initially be deposited via mass wasting occurring as ice cliffs retreated around the lakeshore, causing small landslides of sediments into lakes. As lake area expanded, and sources of sliding debris move further away, sedimentation changes to settling of fines.

Transitions from Facies 1 to Facies 2 require a different explanation. We did not find distinct evidence for this transition in our GPR data, but it was observed in sediment packages associated with a drained lake basin ~60 m north of lake basin A (Fig 2, white hexagon 3; Fig 9, 3). Based on freely available declassified KH-9 and Landsat imagery of the AOI, it can be seen that between 1964 and 1967 a perched lake and backwasting ice cliff located ~60-70 m north in 1964 was expanding and most likely intercepted this location. Throughout the mid-late 1970s the area appears to be submerged but towards the beginning of the early 1980s it is once again exposed. As Spillway Lake began to form and expand, this location was once again submerged, sometime in 2005-2006, and subsequently was re-exposed in the 10/15/2009 Landsat image. A stratigraphic sequence of fine-grained sediments deposited near- parallel with a bare ice surface was exposed over an ice cliff at the lakeshore, indicating deposition onto submerged bare glacier ice. There is an abrupt change from fine sediment to a coarse-grained diamict wedge 1.5 m thick, which extends part way across the underlying fines. Fine-grained material has also been deposited on top of the diamict, supporting the characterization of this sequence in the lake environment, and was the result of a subaqueous debris slumping event (Fig 10).

A conceptual model of supraglacial lake evolution for debris-covered glaciers

Here we present a conceptual model of supraglacial lake evolution, the basis of which is a consolidation of the literature investigating lake formation and expansion, with the addition of the facies relationships observed in our study. Facies transitions suggest that the spatial distribution of debris and depositional processes change as supraglacial lakes grow. These changes reflect varying environmental factors such as proximity to ice cliffs and debris-covered slopes, initiation of calving, interception

with englacial conduits or voids, and subaqueous and subaerial mass movement events. These relationships provide the addition of the evolving debris environment to the model of an expanding supraglacial lake, highlighting the changing debris-related constraints and feedbacks as a supraglacial lake evolves.

During early stages of lake growth, water accumulates in small, isolated lake basins that are perched above base level and not connected to supraglacial streams or englacial conduits (Benn, et al., 2001) (Fig 11, A). The surrounding shoreline likely consists primarily of low gradient, stable debris-covered slopes. Prior to infilling, the lakebed is likely composed of similar diamict as is found above the lake surface (Facies 2). During lake infilling, sedimentation rates in the lake would be low, because sediments would be sourced primarily from windblown dusts or fine-grained materials leached from the surrounding diamict by percolating meltwaters (Facies 1). Consequently, Facies 1 is deposited over Facies 2.

Expansion of small, perched lake basins occurs by slow melting of subaqueous ice around the lake margins, or possibly collapse into englacial voids, which steepens the lakebed slopes, eventually forming steep bare ice faces or ice cliffs (Benn, et al., 2001, Röhl, 2008, Thompson, et al., 2012) (Fig 11, B). Bare ice faces and ice cliffs increase rates of lake expansion and trigger a change in deposition. Bare ice faces often have a thin coating of dark, wet mud which reduces the surface albedo and increases absorption of solar radiation, creating localized hot spots of enhanced melting (Benn, et al., 2001). Ice cliffs can lead to rapid lake expansion through calving, as thermo-erosional notching at the waterline leads to fracturing (Benn, et al., 2001, Röhl, 2008, Miles, et al., 2016). Lake expansion by melt retreat of steep, bare ice faces and calving would cause Facies 2 type sediments to be deposited by

slumping around the expanding lake margin, with deposition of fine-grained Facies 1 sediments in the central deeper areas of the lake.

Sediment deposition can force a positive feedback on lake expansion. Slumping provides a constant influx of diamict, which helps keep turbidity high. This increase in turbidity can decrease lake surface albedo, thereby increasing absorbed solar radiation, which keeps surface temperatures high. Conversely, a negative feedback results from deposited fine sediments (Facies 1) on the lakebed insulating underlying ice from melt, decreasing bottom water cooling. These effects combine to promote melting along lake perimeters, thereby enhancing areal expansion.

Perched lake expansion and sedimentation is halted when lakes intercept englacial conduits or sediment filled crevasse traces and rapidly drain (Fig 11, C) (Benn, et al., 2001, Wessels, et al., 2002, Gulley and Benn, 2007, Röhl, 2008, Benn, et al., 2009, Benn, et al., 2012, Thompson, et al., 2012). While conduits temporarily drain small perched lakes, they play an important role in glacier surface lowering and the development of larger lakes (Kirkbride, 1993, Immerzeel, et al., 2014, Thompson, et al., 2016). Conduit collapse creates new depressions with new bare ice faces where enhanced melting can continue and lakes may eventually be recharged with water from up glacier. In addition, water transported from a lake drainage event loses heat to conduit walls, thereby adding to mass loss through internal ablation (Kirkbride, 1993, Benn, et al., 2012, Miles, et al., 2016, Thompson, et al., 2016) and promotes future collapse by widening conduits (Gulley and Benn, 2007). The presence of Facies 1 in direct contact with glacier ice may be due to a collapse and drainage event that flushed lakebed sediments out of the lake basin, leaving a bare ice surface exposed to melt and sedimentation.

Cycles of lake expansion, drainage by conduits and collapse, and refilling allow smaller, isolated lakes to coalesce behind the terminal moraine to form a large, moraine dammed lake; examples include Imja Tsho, or Tsho Rolpa (Nepal Himalaya) (Fig 11, D-F). While the physical processes driving the change from a series of perched lakes, like Spillway Lake reported here, to a large moraine dammed lake remain poorly understood, it is thought that coalescence of small lakes into a larger one triggers rapid lake expansion through subaerial slab calving, and increased subaqueous waterline melting (Kirkbride, 1993, Sakai, et al., 2009) (Fig. 11, E). While slab calving of exposed ice cliffs can cause rapid lake expansion, deposition of subaerial debris located along the top of ice cliffs onto the lakebed can force a negative feedback on lake expansion (Fig. 11, E). Accumulation of debris at the base of ice cliffs has been observed to separate the ice cliff from the lake, halting calving and lake expansion at that location (Thompson, et al., 2016).

Lake-bed disintegration has been proposed as a key trigger to initiation of full front calving and rapid retreat (Kirkbride, 1993). However, more recent work suggests rapid lake expansion by calving does not require the lake to deepen to the glacier bed (Fig. 11, F). Robertson et al. (2012) observed subaqueous debris layers between 5-10 m in thickness at the calving margins of Mueller, Hooker and Tasman glaciers. Using a CHIRP sonar, they were able to visualize the calving margin where they found a debris-covered sloping ice foot projecting into the lake at an angle of about 40º, indicating the calving front did not reach to the glacier bed (Robertson, et al., 2012). Similarly, a GPR study at Imja Tsho, found glacier ice just up-glacier from the calving front was ~80 m deeper than the deepest point in the lake, indicating that glacier ice was present below the lake bed (Somos-Valenzuela, et al., 2014). Despite debris cover, data from Imja Tsho indicates that some lakebed deepening still

occurs. Taking into consideration that the lake level has been stable for the past decade, at roughly 5010 m a.s.l., the mean rate of deepening at Imja Tsho (2002-2012) was roughly 0.86 my^{-1}, with maximum depths increasing from 98 m to 116 m (Somos-Valenzuela, et al., 2014). Deepening was faster near the calving front and slower nearer the terminus. Some of this deepening may be due to sub-debris melting, but some is due to subaqueous calving (Somos-Valenzuela, et al., 2013, Somos-Valenzuela, et al., 2014).

In summary, using the GPR facies relationships identified in our surveys with field observations, we were able to infer feedbacks between processes controlling supraglacial lake growth and sediment deposition. We have developed a conceptual model of how dominant depositional processes can change as lakes evolve from perched lakes to multi-basin base-level lakes and finally onto large moraine-dammed lakes. Throughout lake evolution, processes such as shoreline steepening, lakebed collapse into voids and conduit interception, subaerial and subaqueous calving and rapid areal expansion alter the spatial distribution and makeup of lakebed debris and sediments which, in turn, can control rates of deepening by enhancing or diminishing heat conduction to the underlying ice.

Conclusion

The results of our GPR surveys not only provide high resolution bathymetric information (beneath the survey lines) allowing us to map the morphology of the lake bed but the additional facies interpretation provided a detailed lakebed debris characterization. This work demonstrates the applicability of GPR as a tool for supraglacial lake investigation and monitoring. We found that lake depth surveys can be completed rapidly with GPR when lake surfaces are frozen. While studies of

supraglacial lakes have traditionally relied primarily on sonar, we showed that GPR provides depth information that is equivalent to sonar, with added information about sediment types on lakebeds. Facies analysis highlights the additional information that can be derived from lakebed surveys using GPR. Sonar data can provide some information about bottom composition, such as surface hardness and texture (Horodyskyj, 2015) but cannot provide the facies information as reported here. Selecting GPR units with CMP survey capability would further expand the utility of GPR, as CMP surveys can provide measurement of the velocity through the debris, allowing the calculation of sediment layer thicknesses, an important parameter for modelling subaqueous heat flux and lake deepening. Further, conducting paired CMP surveys would allow for debris thicknesses to be mapped by determining the material velocity of different facies types, ultimately leading to a much more complete understanding of the spatial distribution, quantity and makeup of lakebed debris.

Future investigations should aim to perform repeat 3-D GPR surveys, which will allow not only detailed changes in lake bathymetry and bed morphology to be measured but also changes in debris distribution. Knowledge such as this is of paramount importance for modelling potential subaqueous lake expansion and understanding the specific thresholds that trigger rapid growth from supraglacial lakes to moraine-dammed lake.

Acknowledgements

Jordan R. Mertes acknowledges funding from Michigan Technological University and The Michigan Technological University 2016 Fall Finishing Fellowship. Sarah S. Thompson acknowledges funding from the University Centre in Svalbard (UNIS) and the European Commission FP7-MC-IEF. We thank Rijan Bhakta Kayastha for

assistance in obtaining research permits, Endra Rai Bahing, Ani Bhattarai and Sujan Bhattarai for logistical support and Lhakpa Nuru Sherpa and the staff at the Cho La Pass Resort for hospitality, logistical support and assistance with fieldwork. We give a huge dhanyabad to Passang Wes for his hard work, without which much of the fieldwork would have been exhausting. We would also like to thank the editor and two anonymous reviewers for constructive reviews that helped us to better organize this manuscript and see it through to fruition.

References

Adhikary S, Nakawo M, Seko K, Shakya B. 2000. Dust influence on the melting process of glacier ice: experimental results from Lirung Glacier, Nepal Himalayas. IAHS PUBLICATION: 43-52

Annan AP, 1992. Ground penetration radar workshop notes. Sensors and Software Inc., Mississauga. p 130, internal report

Annan AP. 2004. Ground penetrating radar principles, procedures and applications

Arcone SA, Finnegan DC, Liu L. 2006. Target interaction with stratigraphy beneath shallow, frozen lakes: Quarter-wave resonances within GPR profiles. Geophysics **71**: K119-K131. DOI: 10.1190/1.2358404

Bajracharya SR, Mool P. 2010. Glaciers, glacial lakes and glacial lake outburst floods in the Mount Everest region, Nepal. Annals of Glaciology **50**: 81-86. DOI: 10.3189/172756410790595895

Banks WSL, Johnson CD, 2011. Collection, processing, and interpretation of ground-penetrating radar data to determine sediment thickness at selected locations in Deep Creek Lake, Garrett County, Maryland, 2007. US Geological Survey

Benn D, Gulley J, Luckman A, Adamek A, Glowacki PS. 2009. Englacial drainage systems formed by hydrologically driven crevasse propagation. Journal of Glaciology **55**: 513-523. DOI: 10.3189/002214309788816669

Benn DI, Bolch T, Hands K, Gulley J, Luckman A, Nicholson LI, Quincey D, Thompson S, Toumi R, Wiseman S. 2012. Response of debris-covered glaciers in the Mount Everest region to recent warming, and implications for outburst flood hazards. Earth-Science Reviews **114**: 156-174. DOI: 10.1016/j.earscirev.2012.03.008

Benn DI, Wiseman S, Hands KA. 2001. Growth and drainage of supraglacial lakes on debrismantled Ngozumpa Glacier, Khumbu Himal, Nepal. Journal of Glaciology **47**: 626-638. DOI: 10.3189/172756501781831729

Benn DI, Wiseman S, Warren CR. 2000. Rapid growth of a supraglacial lake, Ngozumpa Glacier, Khumbu Himal, Nepal. IAHS PUBLICATION: 177-186

Bolch T, Buchroithner M, Peters J, Baessler M, Bajracharya S. 2008. Identification of glacier motion and potentially dangerous glacial lakes in the Mt. Everest region/Nepal using spaceborne imagery. Natural Hazards and Earth System Science **8**: 1329-1340. DOI: 10.5194/nhess-8-1329-2008

Bristow C. 1995. Facies analysis in the Lower Greensand using ground-penetrating radar. Journal of the Geological Society **152**: 591-598. DOI: 10.1144/gsjgs.152.4.0591

Buri P, Pellicciotti F, Steiner JF, Miles ES, Immerzeel WW. 2015. A grid-based model of backwasting of supraglacial ice cliffs on debris-covered glaciers. Annals of Glaciology:

Chikita K, Jha J, Yamada T. 1999. Hydrodynamics of a supraglacial lake and its effect on the basin expansion: Tsho Rolpa, Rolwaling Valley, Nepal Himalaya. Arctic, Antarctic, and Alpine Research: 58-70. DOI: 10.2307/1552623

Chikita K, Jha J, Yamada T. 2001. Sedimentary effects on the expansion of a Himalayan supraglacial lake. Global and Planetary Change **28**: 23-34. DOI: 10.1016/S0921-8181(00)00062-X

Fitzpatrick AAW, Hubbard AL, Box JE, Quincey DJ, Van As D, Mikkelsen APB, Doyle SH, Dow CF, Hasholt B, Jones GA. 2014. A decade (2002–2012) of supraglacial lake volume estimates across Russell Glacier, West Greenland. The Cryosphere **8**: 107-121. DOI: 10.5194/tc-8-107-2014

Fujita K, Sakai A, Nuimura T, Yamaguchi S, Sharma RR. 2009. Recent changes in Imja Glacial Lake and its damming moraine in the Nepal Himalaya revealed by in situ surveys and multi-temporal ASTER imagery. Environmental Research Letters **4**: 045205. DOI: 10.1088/1748-9326/4/4/045205

Gardelle J, Arnaud Y, Berthier E. 2011. Contrasted evolution of glacial lakes along the Hindu Kush Himalaya mountain range between 1990 and 2009. Global and Planetary Change **75**: 47-55. DOI: 727 10.1016/j.gloplacha.2010.10.003

Gardelle J, Berthier E, Arnaud Y. 2012. Slight mass gain of Karakoram glaciers in the early twenty-first century. Nature Geoscience **5**: 322-325. DOI: 10.1038/ngeo1450

Gulley J, Benn DI. 2007. Structural control of englacial drainage systems in Himalayan debris-covered glaciers. Journal of Glaciology **53**: 399-412. DOI: 10.3189/002214307783258378

Haeni F, McKeegan DK, Capron DR, 1987. Ground-penetrating radar study of the thickness and extent of sediments beneath Silver Lake, Berlin and Meriden, Connecticut. In *Water-Resources Investigations Report*. US Geological Survey, WRD

Hands K. 2004. Downwasting and supraglacial pond evolution on the debris-mantled Ngozumpa Glacier, Khumbu Himal, Nepal. University of St Andrews. PHD. http://research-repository.st-andrews.ac.uk/. St. Andrews

Horodyskyj UN. 2015. Contributing factors to ice mass loss on Himalayan debris-covered glaciers. University of Colorado at Boulder. Department of Geological Sciences. Ph.D. 1321773196. http://search.proquest.com/docview/1690497550. UMI Disseratation Publishing

Immerzeel W, Kraaijenbrink P, Shea J, Shrestha A, Pellicciotti F, Bierkens M, De Jong S. 2014. High-resolution monitoring of Himalayan glacier dynamics using unmanned aerial vehicles. Remote Sensing of Environment **150**: 93-103. DOI: 10.1016/j.rse.2014.04.025

Kääb A, Berthier E, Nuth C, Gardelle J, Arnaud Y. 2012. Contrasting patterns of early twenty-first-century glacier mass change in the Himalayas. Nature **488**: 495-498. DOI: 10.1038/nature11324

Kadota T. 1994. Report for the field investigation on the Tsho Rolpa glacier lake, Rolwaling Valley, February 1993–June 1994. WECS Report N **551.489 KAD**:

Kenny A, Cato I, Desprez M, Fader G, Schüttenhelm R, Side J. 2003. An overview of seabed-mapping technologies in the context of marine habitat classification. ICES Journal of Marine Science: Journal du Conseil **60**: 411-418. DOI: 10.1016/S1054-3139(03)00006-7

Kirkbride MP. 1993. The temporal significance of transitions from melting to calving termini at glaciers in the central Southern Alps of New Zealand. The Holocene **3**: 232-240. DOI: 10.1177/095968369300300305

Kirkbride MP, Warren CR. 1997. Calving processes at a grounded ice cliff. Annals of Glaciology **24**: 116-121

Komori J. 2008. Recent expansions of glacial lakes in the Bhutan Himalayas. Quaternary International **184**: 177-186. DOI: 10.1016/j.quaint.2007.09.012

Liu Q, Mayer C, Liu S. 2015. Distribution and interannual variability of supraglacial lakes on debris-covered glaciers in the Khan Tengri-Tumor Mountains. Central Asia. Environ Res Lett **10**: 014014. DOI: 10.5194/tcd-7-4545-2013

Malmberg C, Maryott A. 1956. Dielectric Constant of Water from 0^0 to 1000^0 C. Journal of Research of the National Bureau of Standards **56**: 1-8. DOI: 10.6028/jres.056.001

Miles ES, Pellicciotti F, Willis IC, Steiner JF, Buri P, Arnold NS. 2016. Refined energy-balance modelling of a supraglacial pond, Langtang Khola, Nepal. Annals of Glaciology **57**: 29. DOI: 10.3189/2016aog71a421

Mool P. 1995. Glacier lake outburst floods in Nepal. Journal of Nepal Geological Society **11**: 273-280

Moorman BJ, Michel FA. 1997. Bathymetric mapping and sub-bottom profiling through lake ice with ground-penetrating radar. Journal of Paleolimnology **18**: 61-73. DOI: 10.1023/A:1007920816271

Nakawo M, Rana B. 1999. Estimate of Ablation Rate of Glacier Ice under a Supraglacial Debris Layer. Geografiska Annaler: Series A, Physical Geography **81**: 695-701. DOI: 10.1111/1468-0459.00097

Nicholson L, Benn DI. 2006. Calculating ice melt beneath a debris layer using meteorological data. Journal of Glaciology **52**: 463-470. DOI: 10.3189/172756506781828584

Nicholson L, Benn DI. 2012. Properties of natural supraglacial debris in relation to modelling sub-debris ice ablation. Earth Surface Processes and Landforms. DOI: 10.1002/esp.3299

Østrem G. 1959. Ice melting under a thin layer of moraine, and the existence of ice cores in moraine ridges. Geografiska Annaler **41**: 228-230

Quincey DJ, Luckman A, Benn D. 2009. Quantification of Everest region glacier velocities between 1992 and 2002, using satellite radar interferometry and feature tracking. Journal of Glaciology **55**: 596-606. DOI: 10.3189/002214309789470987

Quincey DJ, Richardson SD, Luckman A, Lucas RM, Reynolds JM, Hambrey MJ, Glasser NF. 2007. Early recognition of glacial lake hazards in the Himalaya using remote sensing datasets. Global and Planetary Change **56**: 137-152. DOI: 10.1016/j.gloplacha.2006.07.013

Reid T, Brock B. 2014. Assessing ice-cliff backwasting and its contribution to total ablation of debris-covered Miage glacier, Mont Blanc massif, Italy. Journal of Glaciology **60**: 3. DOI: 10.3189/2014JoG13J045

Reid TD, Brock BW. 2010. An energy-balance model for debris-covered glaciers including heat conduction through the debris layer. Journal of Glaciology **56**: 903-916. DOI: 10.3189/002214310794457218

Reynolds JM. 2000. On the formation of supraglacial lakes on debris-covered glaciers. IAHS PUBLICATION: 153-164

Reynolds JM. 2011. An introduction to applied and environmental geophysics. John Wiley & Sons

Reznichenko N, Davies T, Shulmeister J, McSaveney M. 2010. Effects of debris on ice-surface melting rates: an experimental study. Journal of Glaciology **56**: 384-394. DOI: 10.3189/002214310792447725

Robertson CM, Benn DI, Brook MS, Fuller IC, Holt KA. 2012. Subaqueous calving margin morphology at Mueller, Hooker and Tasman glaciers in Aoraki/Mount Cook National Park, New Zealand. Journal of Glaciology **58**: 1037-1046. DOI: 10.3189/2012JoG12J048

Röhl K. 2008. Characteristics and evolution of supraglacial ponds on debris-covered Tasman Glacier, New Zealand. Journal of Glaciology **54**: 867-880. DOI: 10.3189/002214308787779861

Ruffell A, Geraghty L, Brown C, Barton K. 2004. Ground-penetrating radar facies as an aid to sequence stratigraphic analysis: application to the archaeology of Clonmacnoise Castle, Ireland. Archaeological Prospection **11**: 247-262. DOI: 10.1002/arp.240

Sakai A, Chikita K, Yamada T. 2000a. Expansion of a moraine-dammed glacial lake, Tsho Rolpa, in Rolwaling Himal, Nepal Himalaya. Limnology and Oceanography **45**: 1401-1408. DOI: 10.4319/lo.2000.45.6.1401

Sakai A, Fujita K. 2010. Formation conditions of supraglacial lakes on debris-covered glaciers in the Himalaya. Journal of Glaciology **56**: 177-181. DOI: 10.3189/002214310791190785

Sakai A, Fujita K, Yamada T. 2005. Expansion of the Imja Glacier Lake in the East Nepal Himalayas. In *Glacier Caves and Glacial Karst in High Mountains and Polar Regions*, Mavlyudov BR (ed). Institute of geography of the Russian Academy of Sciences: Moscow; 74-79

Sakai A, Nakawo M, Fujita K. 2002. Distribution Characteristics and Energy Balance of Ice Cliffs on Debris-Covered Glaciers, Nepal Himalaya. Arctic, Antarctic, and Alpine Research **34**: 12-19. DOI: 10.2307/1552503

Sakai A, Nishimura K, Kadota T, Takeuchi N. 2009. Onset of calving at supraglacial lakes on debris-covered glaciers of the Nepal Himalaya. Journal of Glaciology **55**: 909-917. DOI: 10.3189/002214309790152555

Sakai A, Takeuchi N, Fujita K, Nakawo M. 2000b. Role of supraglacial ponds in the ablation process of a debris-covered glacier in the Nepal Himalayas. IAHS PUBLICATION: 119-132

Sakai A, Yamada T, Fujita K, 2003. Volume change of Imja glacial lake in the Nepal Himalayas. In *Disaster Mitigation & Water Management*: Niigata, Japan

Sambuelli L, Bava S. 2012. Case study: A GPR survey on a morainic lake in northern Italy for bathymetry, water volume and sediment characterization. Journal of Applied Geophysics **81**: 48-56

Sawagaki T, Lamsal D, Byers A, Watanabe T. 2012. Changes in surface morphology and glacial lake development of Chamlang South Glacier, eastern Nepal Himalaya, since 1964. Tokyo. Global Environ Res **16**: 83-94

Schwamborn G, Dix J, Bull J, Rachold V. 2002. High-resolution seismic and ground penetrating radar–geophysical profiling of a thermokarst lake in the western Lena Delta, Northern Siberia. Permafrost and Periglacial Processes **13**: 259-269

Sellmann PV, Delaney AJ, Arcone SA. 1992. Sub-bottom surveying in lakes with ground-penetrating radar.

Shea JM, Immerzeel WW. 2016. Reduced melt on debris-covered glaciers: investigations from Changri Nup Glacier, Nepal. The Cryosphere **10**: 1845. DOI: 10.5194/tc-10-1845-2016

Sneed WA, Hamilton GS. 2007. Evolution of melt pond volume on the surface of the Greenland Ice Sheet. Geophysical Research Letters **34**:

Somos-Valenzuela M, McKinney D, Rounce D, Byers A. 2014. Changes in Imja Tsho in the Mount Everest region of Nepal. The Cryosphere **8**: 1661-1671

Somos-Valenzuela M, McKinney DC, Byers AC, Rounce DR, 2013. Bathymetric survey of Imja Lake, Nepal in 2012. Center for Research in Water Resources, University of Texas at Austin

Thompson S, Benn DI, Mertes J, Luckman A. 2016. Stagnation and mass loss on a Himalayan debris-covered glacier: processes, patterns and rates. Journal of Glaciology: 1-19. DOI: 10.1017/jog.2016.37

Thompson SS, Benn DI, Dennis K, Luckman A. 2012. A rapidly growing moraine-dammed glacial lake on Ngozumpa Glacier, Nepal. Geomorphology **145**: 1-11. DOI: 10.1016/j.geomorph.2011.08.015

Wang W, Gao Y, Anacona PI, Lei Y, Xiang Y, Zhang G, Li S, Lu A. 2015. Integrated hazard assessment of Cirenmaco glacial lake in Zhangzangbo valley, Central Himalayas. Geomorphology. DOI: 10.1016/j.geomorph.2015.08.013

Warren CR, Kirkbride MP. 2003. Calving speed and climatic sensitivity of New Zealand lake-calving glaciers. Annals of Glaciology **36**: 173-178. DOI: 10.3189/172756403781816446

Watanabe T, Kameyama S, Sato T. 1995. Imja glacier dead-ice melt rates and changes in a supra-glacial lake, 1989-1994, Khumbu Himal, Nepal: Danger of lake drainage. Mountain Research and Development: 293-300. DOI: 10.2307/3673805

Watanabe T, Lamsal D, Ives JD. 2009. Evaluating the growth characteristics of a glacial lake and its degree of danger of outburst flooding: Imja Glacier, Khumbu Himal, Nepal. Norsk Geografisk Tidsskrift - Norwegian Journal of Geography **63**: 255-267. DOI: 10.1080/00291950903368367

Wessels RL, Kargel JS, Kieffer HH. 2002. ASTER measurement of supraglacial lakes in the Mount Everest region of the Himalaya. Annals of Glaciology **34**: 399-408. DOI: 10.3189/172756402781817545

Yamada T, Naito N, Kohshima S, Fushimi H, Nakazawa F, Segawa T, Uetake J, Suzuki R, Sato N, Chhetri IK. 2004. Outline of 2002: Research activities on glaciers and glacier lakes in Lunana region, Bhutan Himalayas. Bulletin of Glaciological Research **21**: 79-90

Yamada T, Sharma C. 1993. Glacier lakes and outburst floods in the Nepal Himalaya. IAHS Publications-Publications of the International Association of Hydrological Sciences **218**: 319-330

Tables

Table 1. Processing operations and parameters applied sequentially to profiles of GPR data.

Operation	Parameters
Dewow filter (removal of low-frequency component of trace)	Window length = 80 ns
Static correction (alignment of time-zero in traces)	All first-breaks synchronized to 20.6 ns (= 0.3 m/ns x 6.2 m)
Regularization of trace interval	Trace interpolation to 0.2 m
Normal moveout correction	Assumed velocity = 0.033 m/ns
Ormsby bandpass filter	Corner frequencies = 4-8-50-100 MHz
Constant velocity Kirchhoff migration	Migration aperture = 40 m Velocity = 0.033 m/ns
Median filter	Window = 3 traces x 3 samples
Amplitude gain	Gain function based on constant velocity geometrical spreading correction
Depth conversion	Constant velocity = 0.033 m/ns

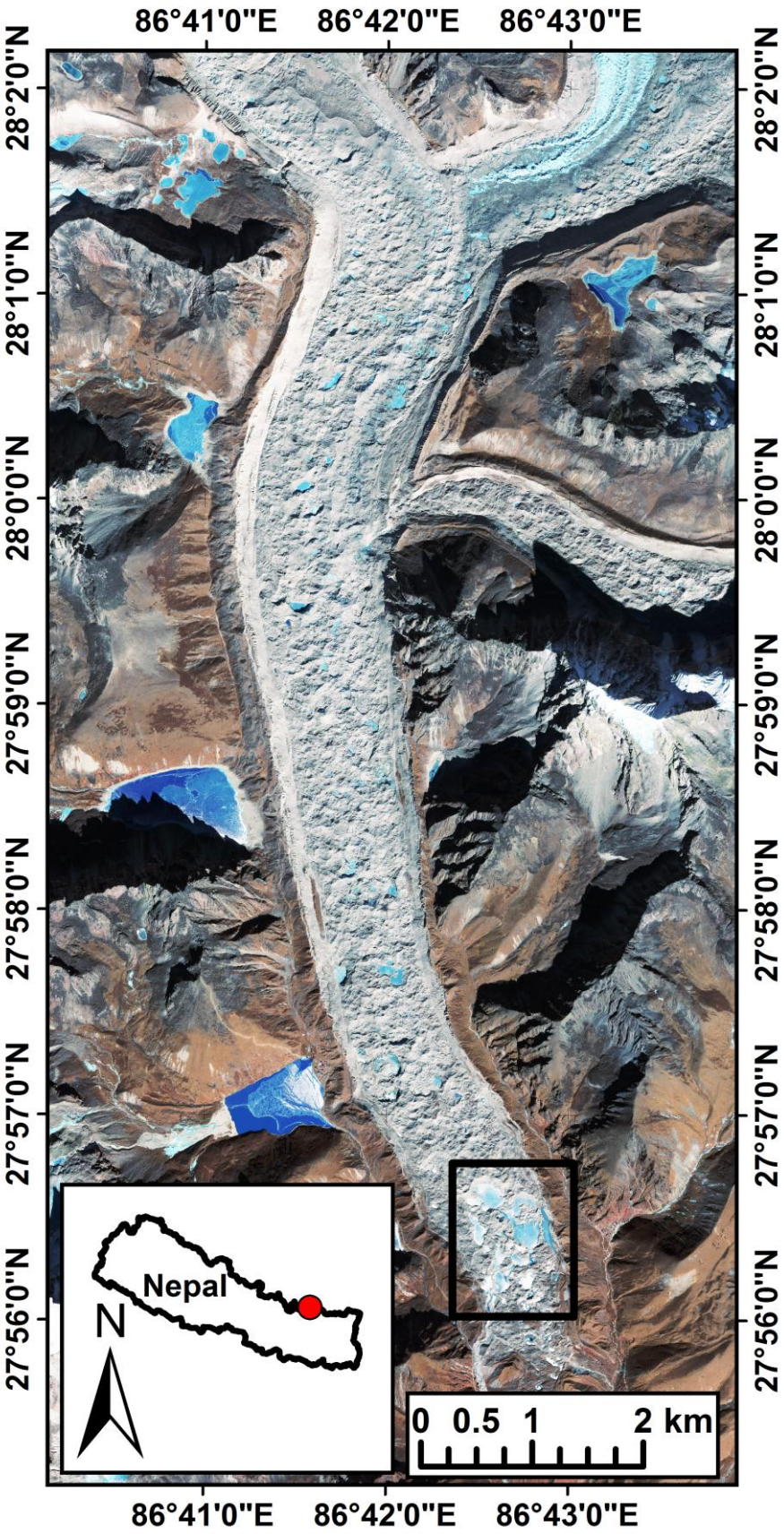

Figure 1: Overview Geoeye satellite image of Ngozumpa Glacier with Spillway Lake complex indicated in black rectangle.

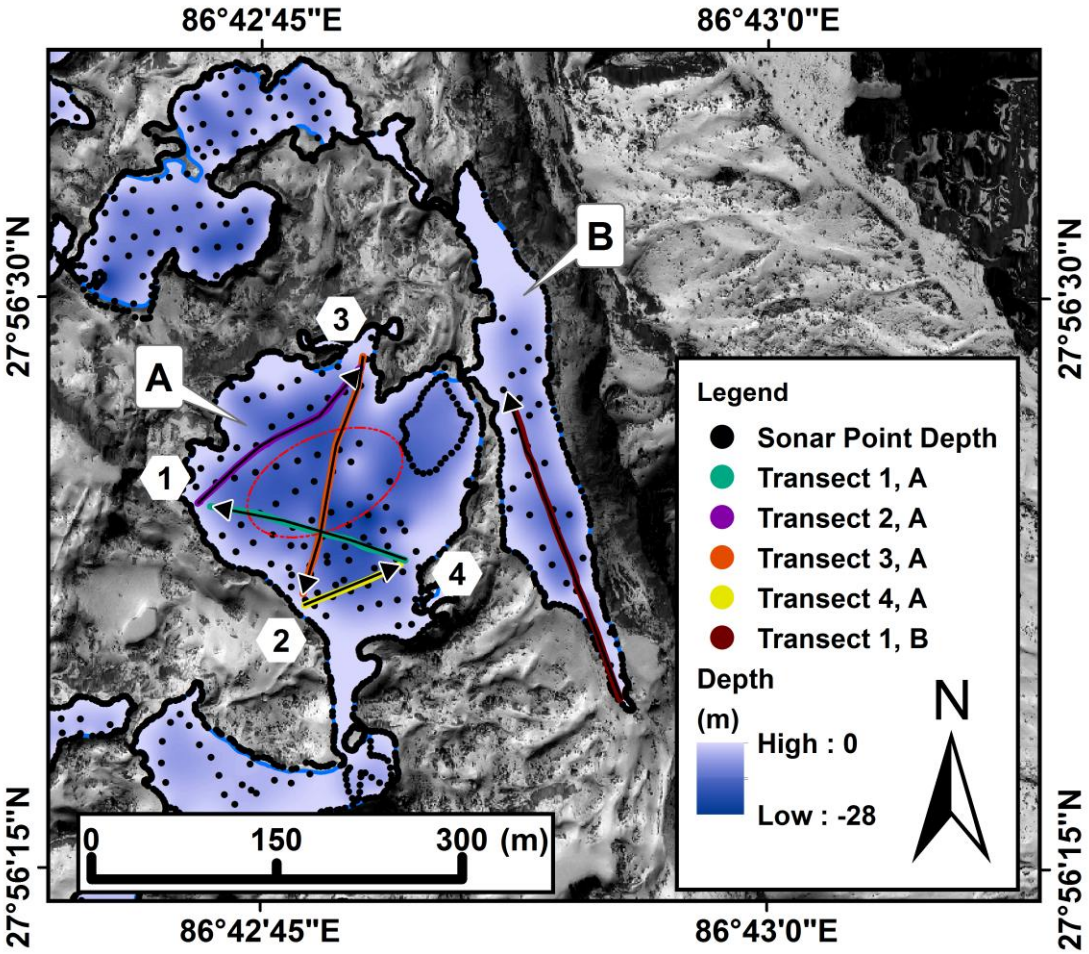

Figure 2: Spillway Lake (basins A & B) area of interest shown with interpolated depth map and overlay of sonar point depth locations and GPR transects. Red ellipse indicates area of sparse sonar point measurements along transect 3, A. White hexagons around numbers indicate locations of sediment samples seen near shoreline in Figures 9&10.

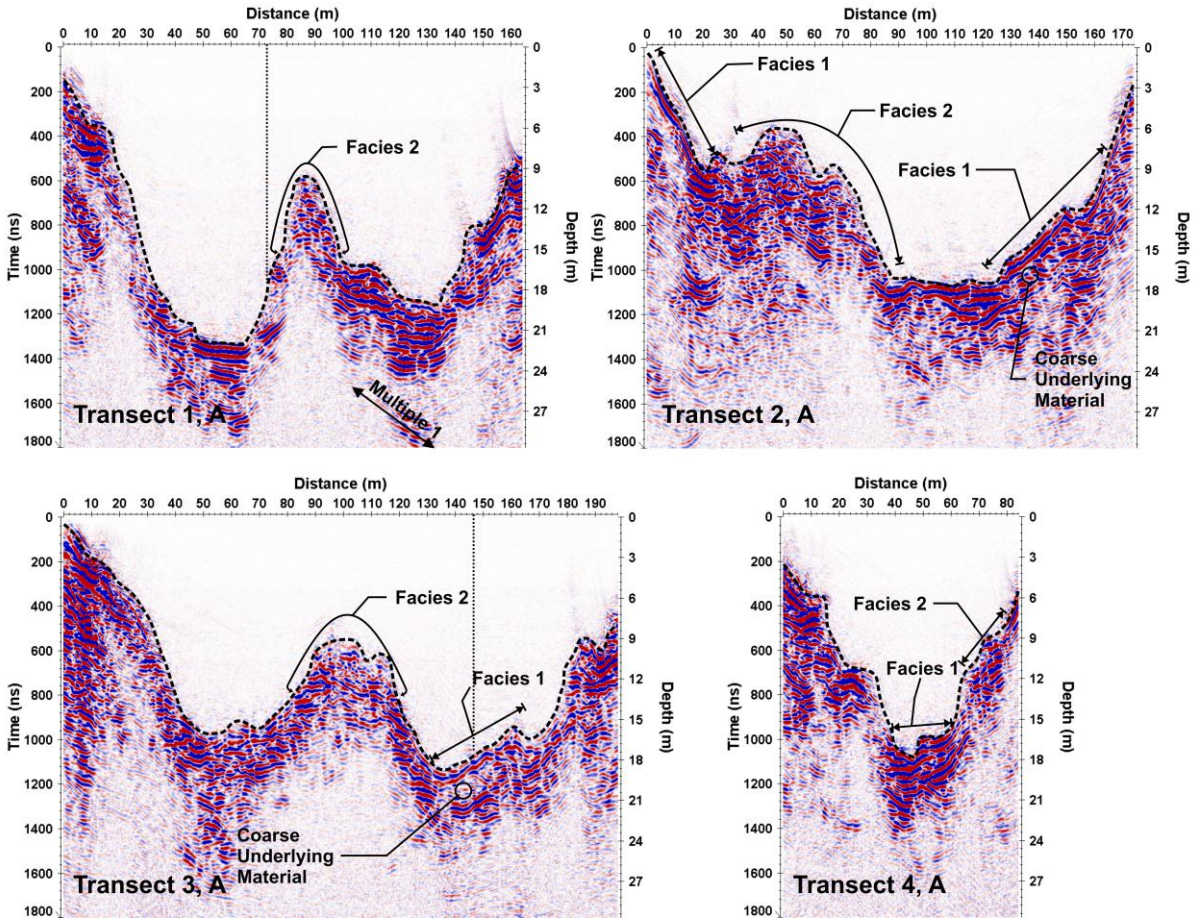

Figure 3: GPR transects 1-4, (basin A), post processed with dashed black line indicating lakebed and labeled multiples and locations of inferred facies. Vertical dotted line indicates crossing point of transects 1 and 3. Vertical exaggeration is roughly 5x. Direction of travel is from left to right.

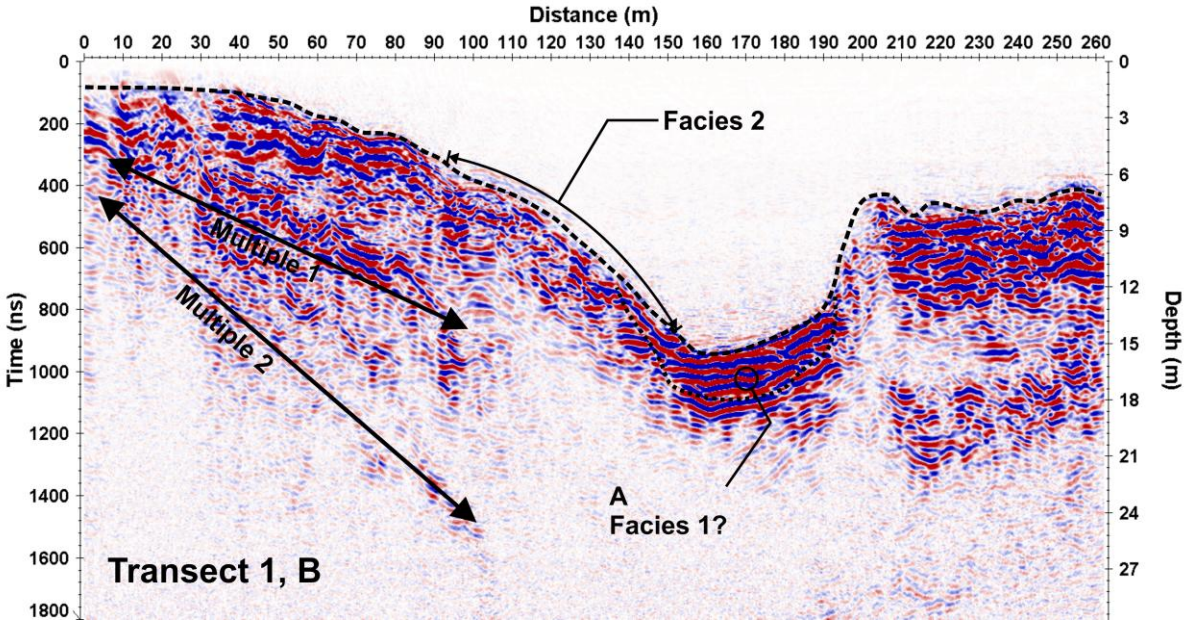

Figure 4: GPR Transect 1, (basin B), post processed with dashed black line indicating lakebed and labeled multiples and locations of inferred facies. Vertical exaggeration is roughly 5x. Direction of travel is from left to right.

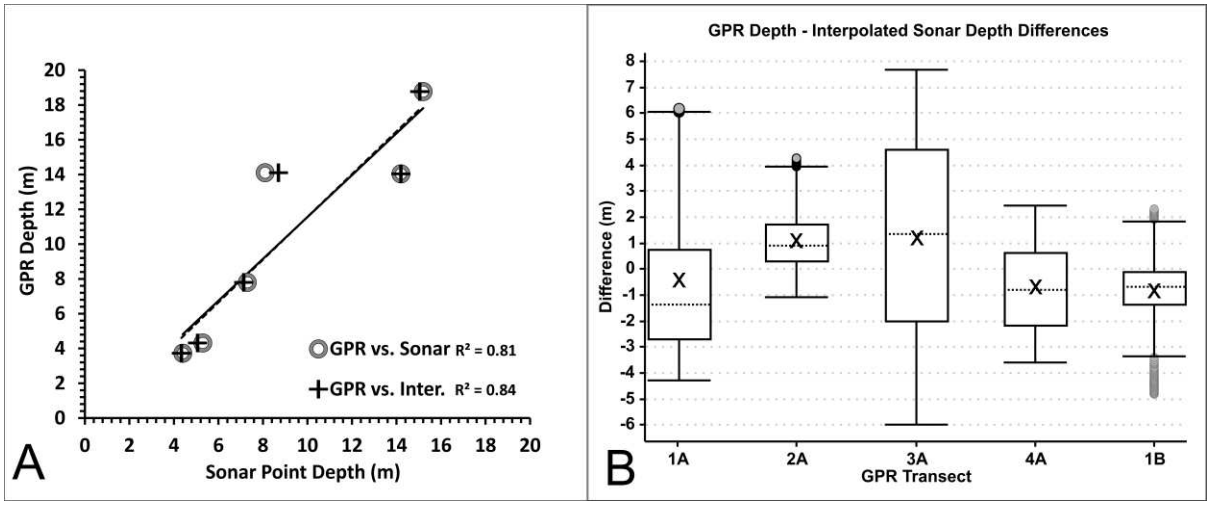

Figure 5: GPR depths compared to sonar point depths and interpolated sonar depth (A). Boxplot of differences between GPR depths and interpolated sonar depth (B). Transects 2A, 4A and 1B display a much smaller interquartile range indicating better agreement between depths, with averages from 1.3 - -1.4m (x).

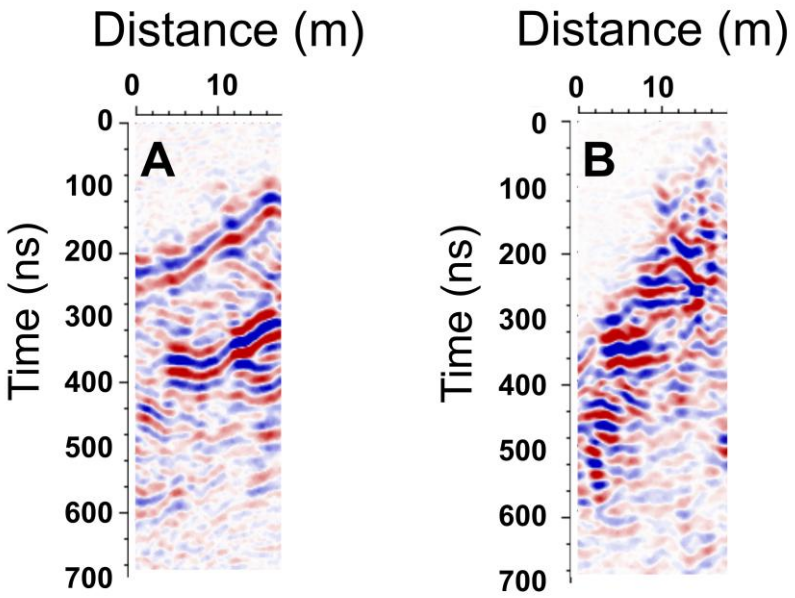

Figure 6: Subsets of distinct radar facies. (A) Coherent, sub-horizontal reflectivity, often comprising subparallel sets of reflections. (B) Typical low-amplitude and chaotic reflectivity, prone to migration noise suggesting structural complexity. Both facies plotted with equivalent amplitude scales.

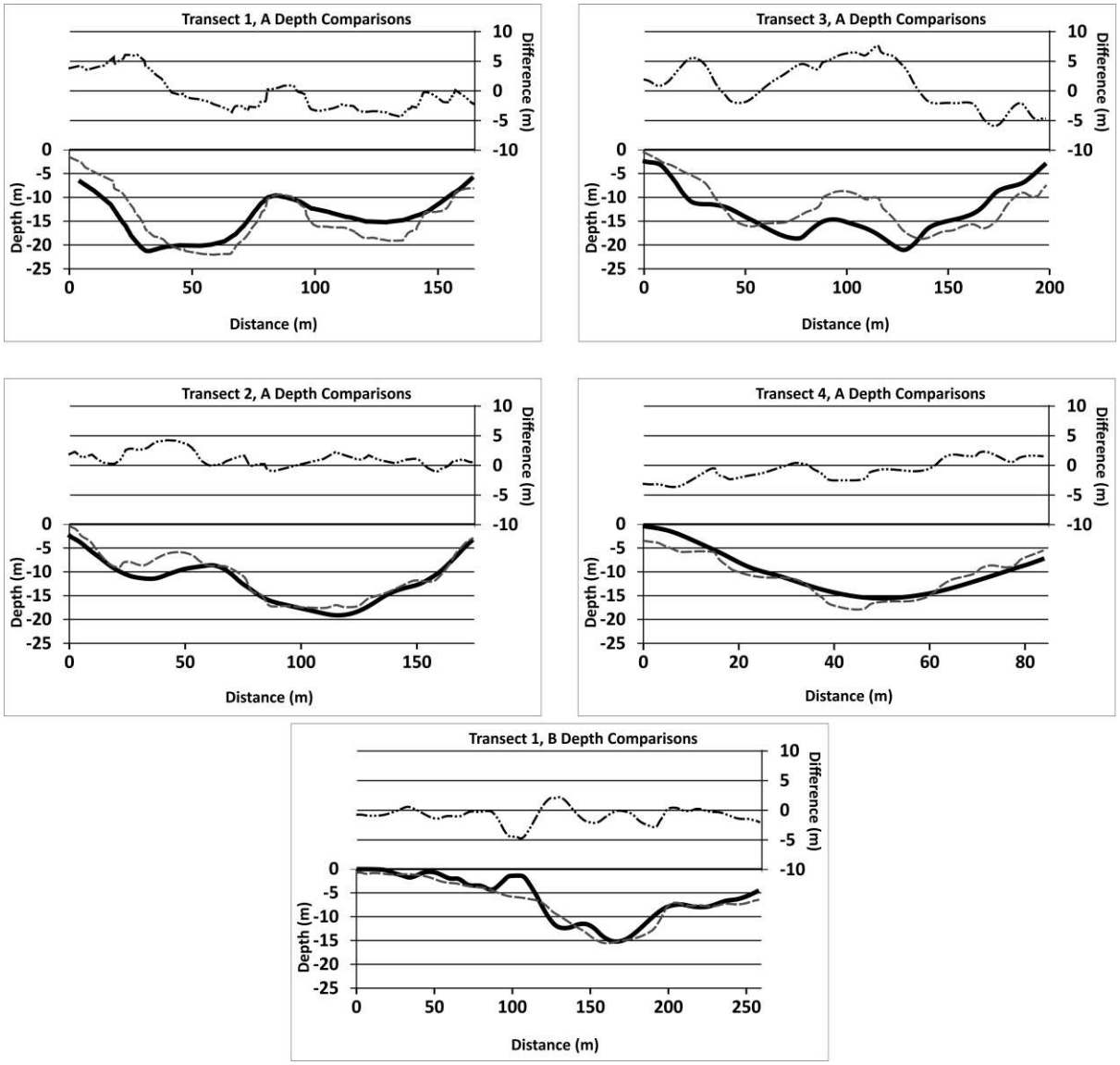

Figure 7: Comparison of GPR depths (gray dashed) and interpolated sonar depths (solid black), with differences (top dash-dot-dot). Note the areas of large difference in transects 1A and 3A, corresponding to areas where there is little overlap between the methods.

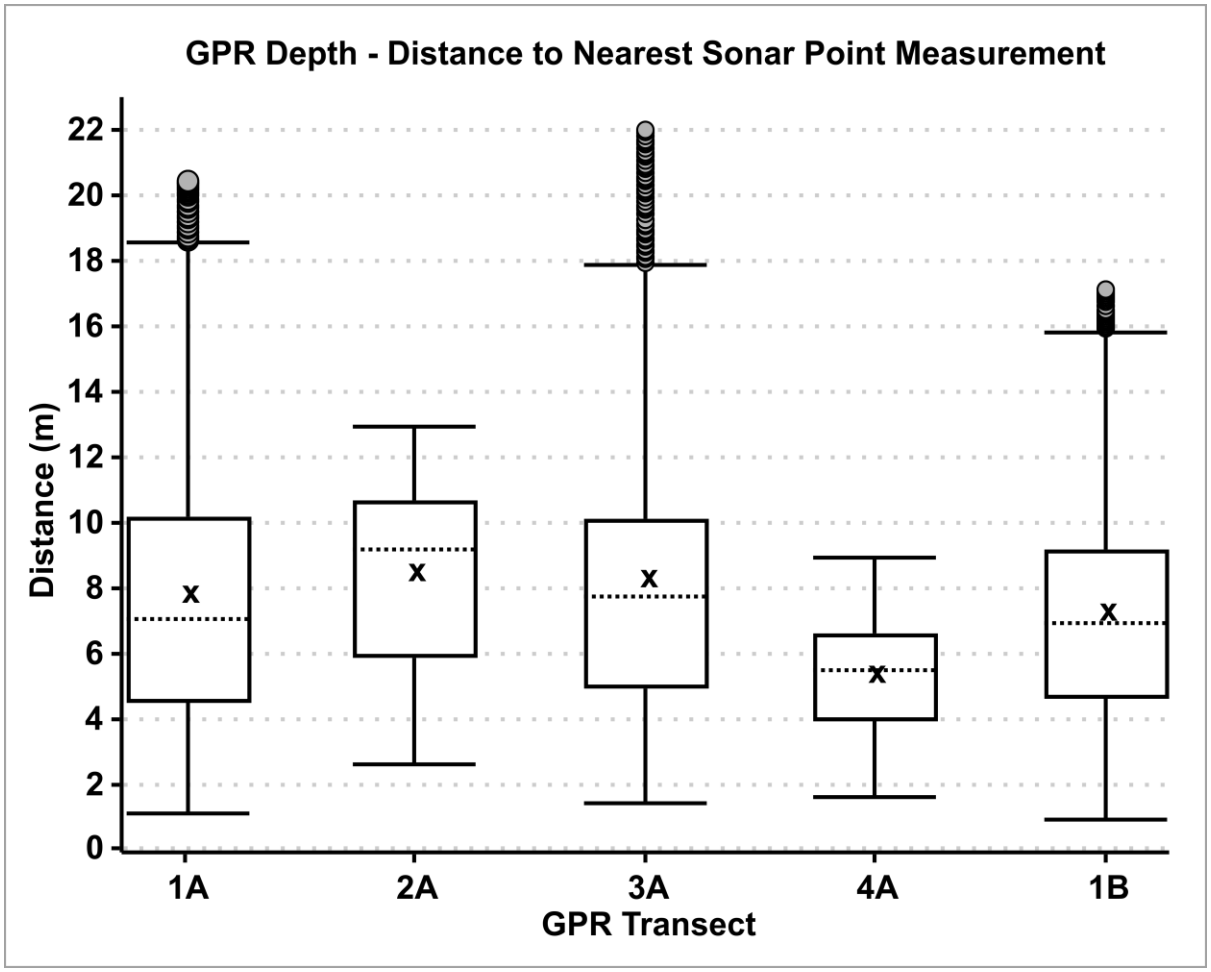

Figure 8: Boxplot of distance from GPR trace to nearest sonar point measurement.

Figure 9: Examples of exposed shoreline facies marked in Figure 2 as white hexagons.

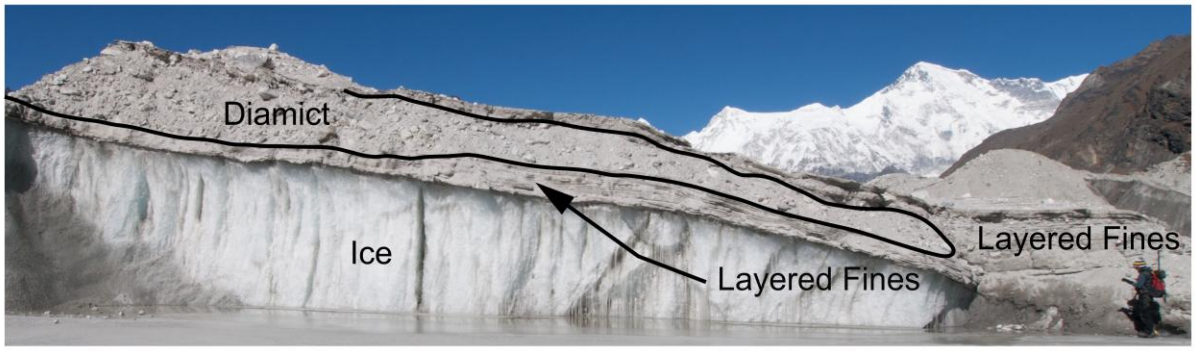

Figure 10: Overview of exposed large diamict wedge deposited between layered fines indicating debris redistribution onto relatively flat, sediment covered lakebed, followed by more fine deposition (Fig 2&9 example 3).

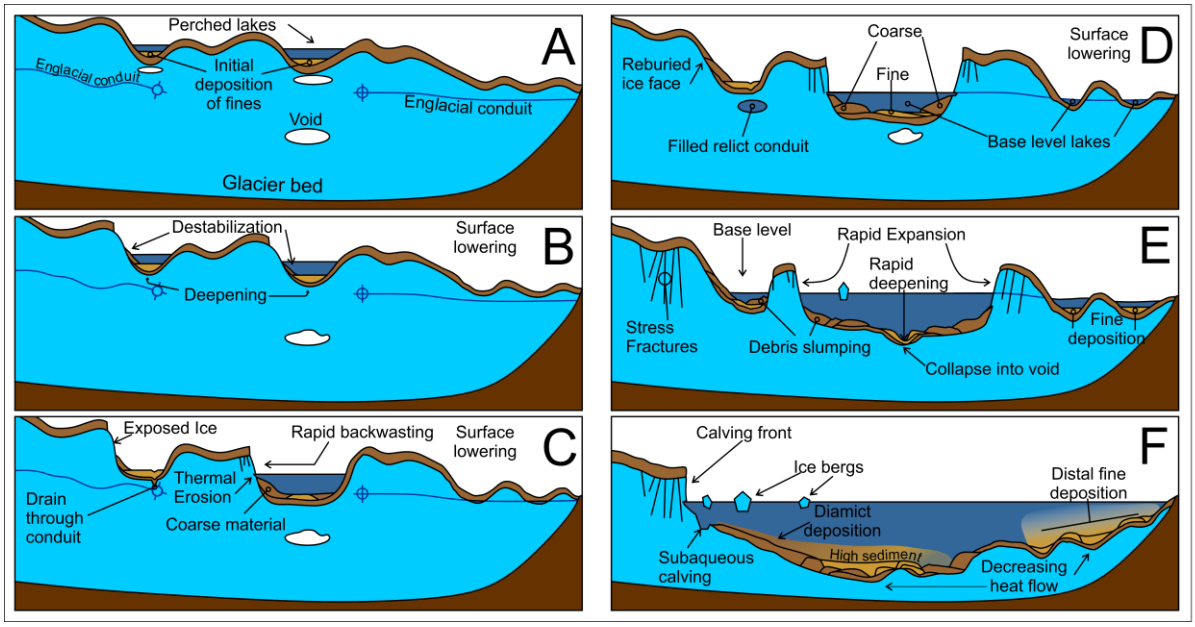

Figure 11: A conceptual model of supraglacial lake evolution on debris covered glaciers with additional changes in sediment depositional processes affecting lakebed spatial debris distribution. (A) Isolated perched lakes, not connected to supraglacial streams or englacial conduits. (B) As perched lakes expand, debris slumping becomes more likely. (C) Some perched lakes may drain due to intersection with englacial conduits, potentially evacuating some lakebed sediment. (D) Ice cliff expansion and lake bed deepening lead to the intersection of the largest lake with a base level conduit. (E) Continued expansion of lakes in the area cause all to connect either through surface drainage networks or near surface conduits. (F) Lake expansion and coalescing leads to the formation of a single base-level moraine dammed lake.